A Near-Infrared Ratiometric Fluorescent Probe for Detecting Endogenous Cu^{2+} in the Brain

Jianping Zhu,[a] Marcus E. Graziotto,[a] Veronica Cottam,[b] Tom Hawtrey[a,c,d], Jourdin R. C. Rouaen,[e] Carolyn Ohno,[f] Marcus Heisler,[f] Orazio Vittorio,[e, g] Kay L. Double,[b] and Elizabeth J. New*[a,c,d]

[a] School of Chemistry, The University of Sydney, Sydney, NSW, 2006, Australia.

[b] Brain and Mind Centre and School of Medical Sciences (Neuroscience), The University of Sydney, Sydney, NSW, 2006, Australia.

[c] Sydney Nano Institute, The University of Sydney, Sydney, NSW, 2006, Australia.

[d] Australian Research Council Centre of Excellence for Innovations in Peptide and Protein Science, The University of Sydney, Sydney, NSW, 2006, Australia.

[e] Children's Cancer Institute, Lowy Cancer Research Centre, University of New South Wales, Sydney, Randwick, New South Wales, Australia.

[f] School of Life and Environmental Sciences, The University of Sydney, Sydney, NSW, 2006, Australia.

[g] School of Biomedical Sciences, University of New South Wales, Kensington, NSW, 2031, Australia.

ABSTRACT

Copper participates in a range of critical functions in the nervous system in the human brain. Disturbances in brain copper content is strongly associated with neurological disease. For example, changes in the level and distribution of copper are reported in neuroblastoma, Alzheimer's disease and Lewy body disorders. There is a need for more sensitive techniques to measure intracellular copper levels to have a better understanding of the role of copper homeostasis in neuronal disorders. Here we report a reaction-based near-infrared (NIR) ratiometric fluorescent probe **CyCu1** for imaging Cu^{2+} in biological samples. High stability and selectivity of **CyCu1** enabled the probe to be deployed as a sensor in a range of systems, including SH-SY5Y and neuroblastoma cells. Furthermore, it can be used in plant cells, reporting copper added to Arabidopsis roots. We also used **CyCu1** to explore Cu^{2+} levels and distribution in postmortem brain tissues from patients with the Lewy body disorder, Dementia with Lewy bodies (DLB). We found significant decreases in Cu^{2+} content in the nuclei, cytoplasm, neurons and extraneuronal space in the degenerating substantia nigra (SN) in DLB compared with healthy age-matched control tissues. These findings enhance our understanding of Cu^{2+} dysregulation in Lewy body disorders. Our probe also shows promise as a photoacoustic imaging agent, with potential for applications in bimodal imaging.

INTRODUCTION

Copper is an essential trace metal vital for human health,[1] and plays a role in a number of important biological processes, including energy metabolism, neuromodulation and antioxidative defense.[2] The redox cycling of copper between oxidized Cu^{2+} and reduced Cu^{+} is key to its roles, particularly as an enzyme cofactor. However, this redox-active nature can generate toxicity through Fenton-like reactions, with the generated reactive oxygen species (ROS) causing oxidative damage to DNA, lipids and proteins.[3] Maintenance of cellular copper homeostasis is therefore of vital to living organisms.

Dysregulation of copper homeostasis is closely associated with neurological conditions including, but not limited to, Wilson's disease, Alzheimer's disease, Parkinson disease and neuroblastoma.[2] Though it is still debatable whether copper dyshomeostasis is a cause, or consequence, of some of these conditions, there is strong evidence for an aetiological role for copper in a number of these diseases. Studies in Wilson's disease, a genetic disorder resulting in brain copper accumulation, suggest that when the copper content exceeds the binding capacity of cellular glutathiones and metallothioneins, the subsequent increase in oxidative stress results in cell damage.[2] Copper is an essential cofactor in antioxidants, such as superoxide dismutase 1 (SOD1), and the brain copper deficiency observed in Parkinson disease is proposed to impair ROS removal, leading to elevated oxidative

stress.[4]

The distribution of copper in the human brain is heterogeneous. In the healthy brain, high copper content is found in the catecholaminergic locus coeruleus and substantia nigra,[5] brain regions vulnerable in Parkinson disease where these regions experience a decrease in copper of 55% compared with those in healthy brains.[6] In Alzheimer's disease patients, copper levels are up to 50% lower in the hippocampus, frontal cortex, cerebral cortex and amygdala compared with healthy controls,[3, 7] but higher in amyloid plaques.[8]

Dementia with Lewy bodies is a common dementia disorder exhibiting some symptoms and pathologies characteristic of both Alzheimer's disease and Parkinson disease. Probable DLB is diagnosed on the basis of clinical features and indicative biomarkers.[9] Pathological mechanisms in DLB are, however, poorly understood and pharmacological treatments have limited efficacy.[10] Identifying molecular biomarkers and metabolic alterations in the brains of individuals with DLB may advance the development of more effective symptomatic treatments, or disease-modifying therapies, for DLB. While changes in brain copper levels are associated with Alzheimer's disease and Parkinson disease, as described above, brain copper levels in DLB have not previously been reported.

Neuroblastoma is the third most common cancer in the childhood, with low survival rates of 40–50% in high risk patients, even with therapy.[11] Elevated copper levels in tumor and patient's blood are correlated to increased aggressiveness and progression of neuroblastoma disease.[12] Members of our team have been reported that copper levels in neuroblastoma cell lines are 50% higher than normal human fibroblasts.[13]

Over the past decade, quantification of brain tissue copper content has primarily employed biophysical techniques, such as inductively-coupled plasma mass spectrometry (ICP-MS),[5a] which requires destructive digestion of the tissue sample before measurement. Synchrotron radiation X-ray fluorescence microscopy (SRXFM) and particle induced X-ray emission (PIXE) microscopy have been used to quantify copper levels at the single cell level in tissue sections in Parkinson disease brain.[6] All these techniques measure total copper content; that is, the sum of protein-bound copper and labile copper, and are not able to distinguish one from the other. It is likely that the majority of copper in the brain is bound to a variety of molecules, such as copper transport proteins, cuproproteins and the metal-binding pigment neuromelanin,[6, 14] but it is the labile, or bioavailable, copper pool that most strongly determines the pathological effects of copper, and yet such changes in labile copper have not been so widely explored in neurological conditions.

To maintain tightly copper homeostasis, cells contain an array of proteins involving in copper import, chaperoning, and export.[15] Several copper transporters have been identified. High-affinity copper transporter 1 (Ctr1) dominates copper transport, while copper transporter 2 (Ctr2) and divalent metal transporter DMT1 also mediate copper import into cells.[16] Cu^{+} is thought to be the predominant species in cells instead of Cu^{2+} as a result of a reductive intracellular environment. The conventional view is that Cu^{2+} is reduced to Cu^{+} by metalloreductases outside the cell and it is Cu^{+} that is then imported by those transporters.[17] However, there is no direct evidence for the absence of intracellular Cu^{2+}. One possibility is that transient Cu^{2+} ions exist in cells, but are too short-lived to be detected. Fluorescent probes have been shown to be an effective tool for the detection of metal species in cellular environment, exhibiting the advantages of high sensitivity and selectivity while also providing spatiotemporal information about the analytes. Recently, the Chang group developed a fluorescent probe CD649.2 selective for Cu^{2+} which was combined with the Cu^{+}-selective probe CF4 to investigate cellular copper transport.[18] These authors demonstrated that DMT1 imports Cu^{2+} ions, complementing the Cu^{+} transport by Ctr1.

Fluorescent Cu^{2+} probes are less commonly applied to biological studies compared to Cu^{+} probes. It is not straightforward to prepare binding-based probes for Cu^{2+}, where the fluorescence change results from electronic interactions between the probe and the analyte. This is because Cu^{2+}, with its $3d^{9}$ electron configuration, has the

potential to quench fluorescence emission due to its paramagnetic nature.[19] Moreover, Cu^{2+} is classified as a borderline Lewis acid, along with the main essential transition metals, such as Zn^{2+} and Fe^{2+},[20] making it difficult to sense Cu^{2+} with high selectivity. To make fluorescent probes that have unique selectivity for Cu^{2+} and avoid a quenched fluorescence response, sophisticated probe designs are required. In contrast, activity-based fluorescent probes generate a fluorescence response from a change in their chemical structure upon reacting with the analytes. This sensing mechanism enables the detection of analytes with high specificity. Furthermore, the analyte dissociates from the fluorescent dye after the reaction, thus avoiding quenching by paramagnetic metal ions.

NIR fluorescence excitation and emission diminish photodamage to living cells and minimize light scattering through tissues, which is beneficial for biological applications.[21] Ratiometric fluorescent probes measure changes in the ratio between two emission bands upon response to analytes. This self-calibration minimizes analyte-independent interferences, such as instrument parameters, photobleaching, probe concentrations and the complex cellular or tissue environment.[22] We aimed to develop a reaction-based NIR ratiometric fluorescent probe for Cu^{2+} that addresses these considerations. Several NIR ratiometric fluorescent probes for Cu^{2+} have been reported, but these probes only detect exogenous Cu^{2+} in either mammalian cells or mice.[23] Fluorescent probes for detecting endogenous Cu^{2+} are less frequently reported, especially for investigation of regional or cellular variations of Cu^{2+} levels in neurological conditions. We have therefore applied our Cu^{2+} probe to exploring Cu^{2+} levels in two neurological diseases characterized by copper dyshomeostasis.

RESULTS AND DISCUSSION

Design and synthesis of CyCu1. To generate a selective response towards Cu^{2+}, a specific reaction site needs to be installed onto fluorescent dyes. It has been reported that Cu^{2+} catalyzes the hydrolysis of the ester bond in 2-picolinate ester derivatives (Figure 1a).[24] The complexation of Cu^{2+} with the pyridine N and carbonyl O enhances the electrophilicity of the carbonyl group. This promotes the nucleophilic attack by H_2O at the carbonyl, accelerating the hydrolysis of the ester.[24] This reaction can be used as a sensing mechanism for Cu^{2+}, which has been demonstrated by an aza-BODIPY based photoacoustic probe for Cu^{2+}.[25] The reactive functional group, 2-picolinate ester has been used in a few cases of copper sensing.[26] We chose commercially available IR-780, a cyanine derivative with good biocompatibility,[27] as the NIR fluorescent scaffold (Scheme S1). 2-Picolinate ester was installed onto the cyclohexene moiety, giving probe **CyCu1** (Figure 1a). In response to Cu^{2+}, the 2-picolinate ester in **CyCu1** was expected to hydrolyze to an alcohol, which would undergo a tautomerism to the ketone CyK1 (Figure 1a). This results in dramatic changes in the electron conjugation in the molecule. Consequently, we expected both absorption and fluorescence emission wavelength to shift. The change in absorption provides potential for the probe to be used in photoacoustic imaging of Cu^{2+}. Probe **CyCu1** was synthesized in two steps (Scheme S1). First, a solution of IR-780 in DMF was treated with NaAc, converting IR-780 to the ketone CyK1 in 56% yield. 2-Picolinate acid was then coupled to CyK1 with coupling reagents EDC·HCl and DMAP, giving **CyCu1** in 50% yield.

Photophysical properties. The photophysical properties of **CyCu1** and its response to Cu^{2+} were characterized in HEPES buffer (20 mM, pH 7.4). **CyCu1** gave a maximum absorption at 784 nm with a shoulder peak at 720 nm (Figure 1b). Upon addition of five equivalents of Cu^{2+}, the absorption band blue-shifted to 526 nm (Figure 1b). CyK1 also exhibited a broad absorption band showing the same peak shape and centered at 526 nm (Figure S1), suggesting that **CyCu1** does indeed convert to CyK1 after reaction with Cu^{2+}. This is consistent with our assumption that the 2-picolinate ester group in **CyCu1** was hydrolyzed and the intermediate then tautomerized to CyK1 (Figure 1a).

We then turned to investigation of the fluorescence properties of **CyCu1** and CyK1 (Figure S2). **CyCu1** exhibited a maximum excitation at 792 nm, and its maximum emission was located at 810 nm (Figure S2a). The NIR excitation and emission makes **CyCu1** promising for *in vivo* imaging. Due to the narrow Stokes shift of **CyCu1** (18 nm), and to enable us to record an intact emission spectrum, **CyCu1** was excited at 710 nm in subsequent studies. The excitation spectrum of CyK1 was in the visible region, with a maximum excitation at 523 nm, and its maximum emission was at 600 nm (Figure S2b). Since the maximum excitation wavelengths of **CyCu1** and CyK1 were 269 nm apart, it was necessary to excite **CyCu1** at these two different wavelengths, 523 and 710 nm, in order to observe both probe and product. After adding five equivalents of Cu^{2+} to a solution of **CyCu1**, the fluorescence emission underwent a hypsochromic shift to 600 nm (Figure 1c), corresponding to the fluorescence emission spectrum of CyK1. This fluorescence study further confirmed that **CyCu1** converted to CyK1 in response to Cu^{2+}.

The sensing mechanism of **CyCu1** for Cu^{2+} was also investigated using mass spectrometry (Figure S3). Solutions of CyK1 and **CyCu1** in the absence and presence of five equivalents of Cu^{2+} were prepared in a mixture of H_2O and CH_3OH (1:1, v/v), and the solutions were incubated at rt for 4 h. **CyCu1** exhibited a m/z peak at 626.4 (Figure S3a). In the presence of Cu^{2+}, **CyCu1** gave a m/z peak at 521.5 (Figure S3b), matching to the peak of CyK1 (Figure S3c).

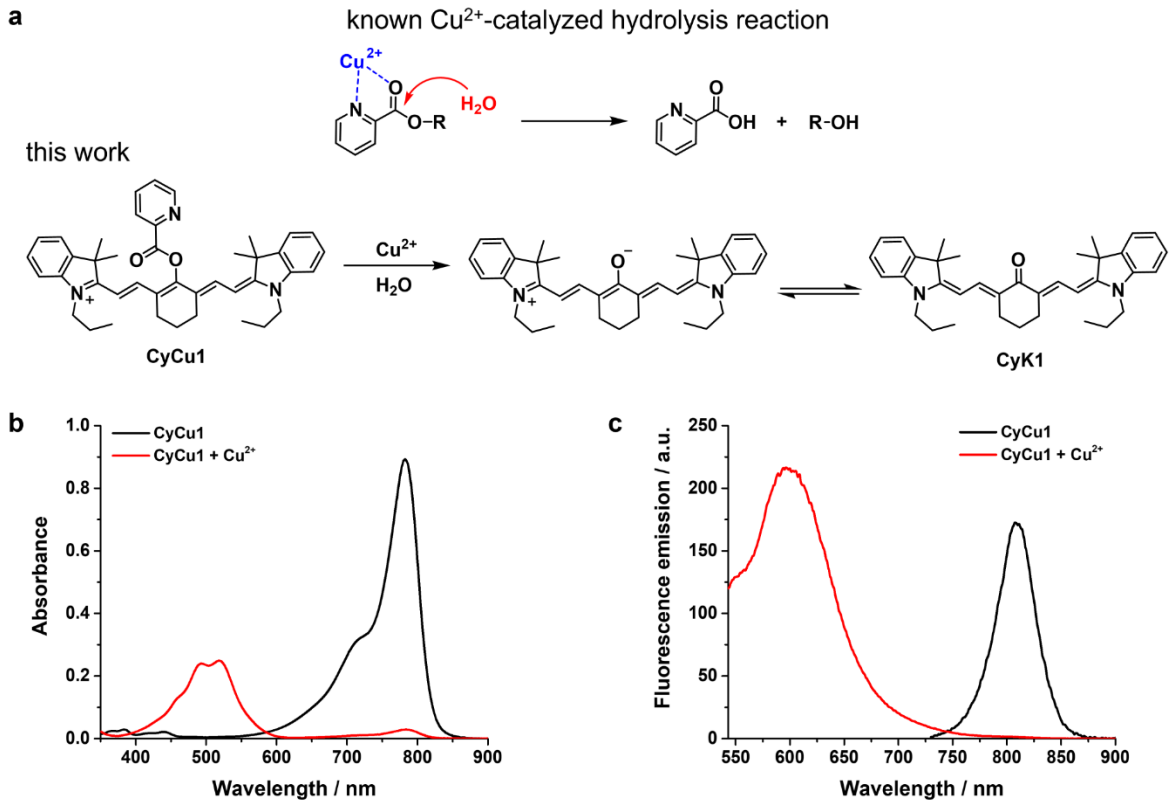

Figure 1. (a) The mechanism of Cu^{2+}-catalyzed hydrolysis of 2-picolinate ester and proposed sensing mechanism of **CyCu1** for Cu^{2+} in this work. (b) Absorption spectra of **CyCu1** (10 μM) in the absence and presence of five equivalents of Cu^{2+} in HEPES buffer (20 mM, pH 7.4, containing 1% DMSO and 0.1% CrEL as cosolvents, v/v). (c) Fluorescence emission spectra of **CyCu1** (5 μM) in the absence (λ_{ex} = 710 nm) and presence (λ_{ex} = 523 nm) of five equivalents of Cu^{2+} in the HEPES buffer.

The stabilities of **CyCu1** and CyK1 in aqueous solution were explored by recording their fluorescence emission

spectra at times up to 75 min (Figure S4). **CyCu1** exhibited stable emission at 810 nm over time with excitation at 710 nm (Figure S4d), with negligible emission when excited at 523 nm (Figure S4b), indicating that **CyCu1** had good stability in the aqueous working solution. CyK1 was also stable in the solution as shown by its steady emission at 605 nm (Figure S4a, c). Good stability was also observed by absorption (Figure S5a, b).

The time-course fluorescence response of **CyCu1** to Cu^{2+} was next recorded (Figure S6). After adding five equivalents of Cu^{2+}, the emission of **CyCu1** at 810 nm gradually decreased over time (Figure S6b), while the emission at 605 nm increased (Figure S6a). The response of **CyCu1** towards Cu^{2+} reached to saturation in 40 min (Figure S6c, d), with the same time profile also observed by absorption (Figure S5d, e)

Having demonstrated that **CyCu1** is stable in HEPES buffer at pH 7.4, its stability in HEPES buffer at different pH values was explored. The absorption spectra of **CyCu1** in acidic, neutral and basic conditions were recorded over 50 min (Figure S7a–f). No significant variations in the absorbance at different pH values were observed, and the changes in the absorbance after 50 min were negligible, demonstrating that pH did not affect the stability of CyCu1 in aqueous solution (Figure S7g). The rate constant of the transformation of **CyCu1** to CyK1 with the Cu^{2+} catalysis was calculated using a pseudo first-order plot[28] and the pseudo first-order rate constant was calculated to be 0.094 min^{-1} (Figure S8). Since the reaction rate of fluorescent Cu^{2+} probes is rarely reported, the rate of **CyCu1** response to Cu^{2+} cannot be readily compared to those of other Cu^{2+} probes.

Titration of **CyCu1** with Cu^{2+} showed a ratiometric response to Cu^{2+} addition, with the emission at 600 nm increasing (Figure 2a) while the emission at 810 nm decreased (Figure 2b). There were corresponding absorption changes: the absorbance at 782 nm reduced while the absorbance at 518 nm increased (Figure 2c), demonstrating a clear colorimetric change from cyan to orange. The limit of detection was measured to be 0.053 μM (Figure S9). The reported copper levels in the tissue of patients varies significantly in different cancers, such as 0.06 μM in ovarian cancer, 0.312 μM in stomach cancer and 2.68 μM in breast cancer.[29] The reported copper content in SK-N-BE(2)-C neuroblastoma cell lines is about 48 μM/mg protein[30] while the reduced copper levels in the Parkinson's locus coeruleus was determined to be 30 μg/g dry weight.[6] While not all of these values can be directly compared with the limit of detection for our probe, the low limit of detection of **CyCu1** suggests it could be useful for measuring copper in a range of diseases in which this metal has been implicated.

The selectivity of **CyCu1** for Cu^{2+} over a variety of metals was investigated (Figure 2d, S10). No metals other than Cu^{2+} gave significant changes in both fluorescence emissions (Figure 2d, S10a, b), demonstrating that **CyCu1** exhibited good selectivity for Cu^{2+}. Further addition of Cu^{2+} to the mixture of **CyCu1** and other metals dramatically reduced the emission at 810 nm (Figure S11b, c), and remarkedly increased the emission at 600 nm (Figure S11a, c), verifying that **CyCu1** was capable of detecting Cu^{2+} in the presence of other metals. The change in absorption spectra of **CyCu1** upon treatment with metals further indicated good selectivity of **CyCu1** for Cu^{2+} (Figure S12). Among various metals, only Cu^{2+} led to the hypsochromic shift from 782 nm to 518 nm, demonstrating that **CyCu1** can selectively report on Cu^{2+} colorimetrically. The coordination of Cu^{2+} to pyridine N and carbonyl O in the picolinate ester is crucial for the acceleration of the hydrolysis reaction. Other metals might not bind tightly to these two sites, and they are therefore not able to catalyze the hydrolysis of the ester.

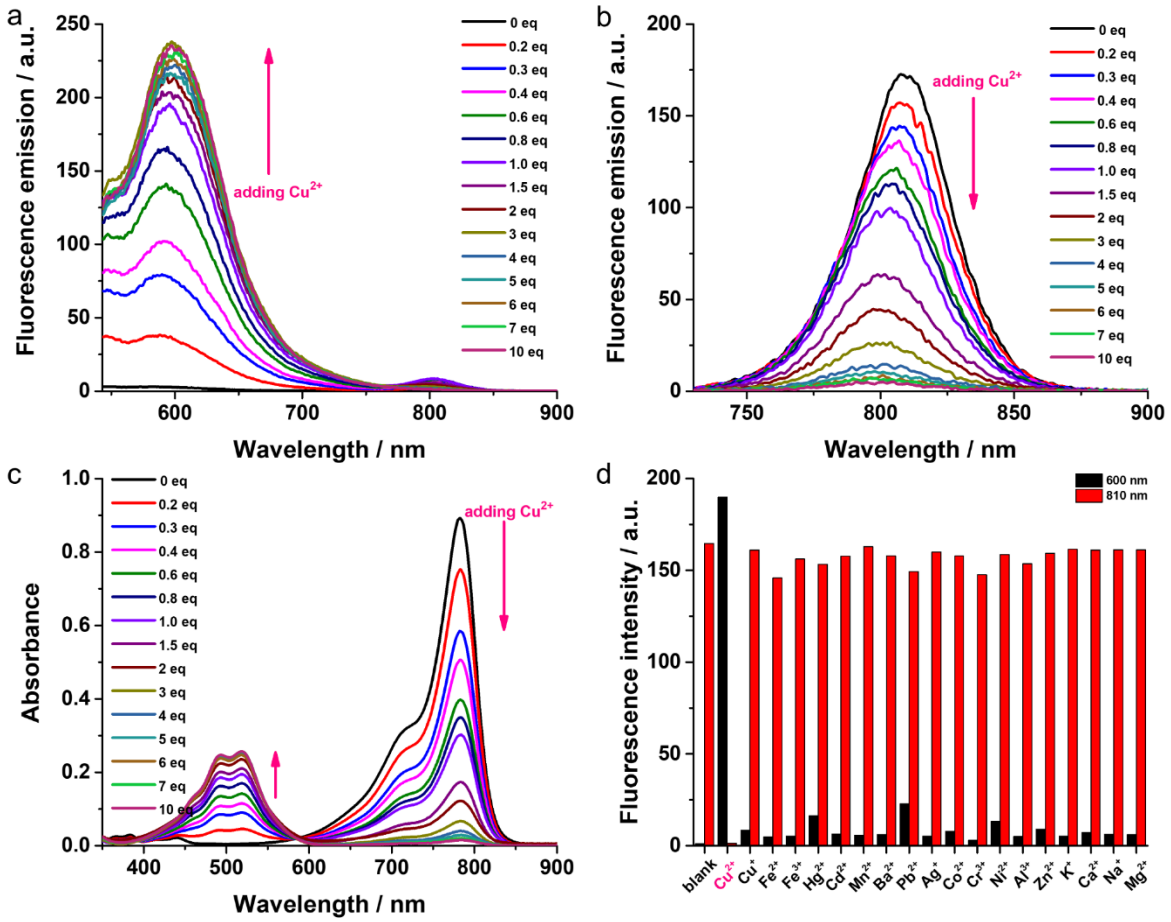

Figure 2. Different concentrations of Cu^{2+} were added to a solution of **CyCu1** (5 μM) in HEPES buffer (20 mM, pH 7.4, containing 0.5% DMSO and 0.1% CrEL as cosolvents, v/v) and incubated at rt for 1 h before collecting fluorescence emission and absorption spectra. (a, b) Fluorescence emission spectra excited at (a) 523 nm and (b) 710 nm. (c) Absorption spectra. (d) Selectivity of **CyCu1** for metals. A variety of metals (100 equivalents for K^+, Ca^{2+}, Na^+ and Mg^{2+}, five equivalents for other metals) were added to a solution of **CyCu1** (5 μM) in the HEPES buffer and incubated for 1 h at rt. Fluorescence spectra were then recorded with excitation at 523 nm and 710 nm (Figure S10) and fluorescence intensities at 600 nm and 810 nm were measured.

Based on the good stability of **CyCu1** and excellent selectivity for Cu^{2+}, we sought to apply the probe to cellular and tissue imaging of Cu^{2+}. Two fluorescence emission channels were collected in the confocal imaging in the following studies: CH1 (580–650 nm) for the product CyK1 and CH2 (750–800 nm) for the probe **CyCu1**.

Cellular study. CyCu1 was first applied to the imaging of Cu^{2+} in SH-SY5Y cells. SH-SY5Y is a thrice-subcloned neuroblastoma cell line derived from SK-N-SH lineage and serves as a cell model for *in vitro* studies of neurodegenerative disorders, eg. Parkinson disease.[31] Cell viability of SH-SY5Y cells were determined by Alamar Blue assay, suggesting that both **CyCu1** and CyK1 were non-toxic to the cells at 10 μM after treatment for 24 h (Figure S13). Both the probe and the product exhibited good biocompatibility at low concentrations. Intense fluorescence was observed in both channels in cells treated with **CyCu1** for 1 h (Figure 3a–d), indicating that **CyCu1** was able to penetrate through the cell membrane and a fraction of **CyCu1** was converted to CyK1 in the cellular environment. Another group of cells was pretreated with Cu^{2+}(ATSM) for 1 h, an exogenous Cu^{2+} source,[32] followed by incubation with **CyCu1** for 1 h. Fluorescence emissions were detected in both channels, with an

increased intensity ratio between CH1 and CH2 when compared to that of cells only treated with **CyCu1** (Figure 3e–h, m). This result suggested that **CyCu1** was able to detect exogenous Cu^{2+}. Negligible fluorescence was observed in cells treated with CyK1 for 1 h (Figure 3i–l), indicating that CyK1 was not cell permeable. The difference of CyK1 and **CyCu1** in cell permeability can be attributed to their charge. **CyCu1** is positively charged, while CyK1 is neutral charge. The positive charge enables **CyCu1** easy to be taken up into cells, while neutral compounds usually suffer from poorer cell permeability.[33]

An emission spectral scan was conducted to verify whether the cellular fluorescence came from the probe **CyCu1** or the product CyK1. An emission spectral scan of cells treated with **CyCu1** for 1 h with two-photon excitation at 840 nm showed a strong emission peak at 790 nm, with a small peak at 610 nm (Figure 3n). To determine whether the emission at 610 nm came from CyK1, a spectral scan of CyK1 was conducted in PBS with the same excitation, and was found to have a maximum emission at 610 nm (Figure S14). This evidence supported that in the cellular environment, the probe mainly existed in the form of **CyCu1** and a small fraction as CyK1. In cells pretreated with Cu^{2+}(ATSM) then with **CyCu1**, intense emission peaks were detected at 610 nm and 790 nm and the ratio of the intensity between the two peaks was remarkably larger than that of the cells treated with **CyCu1** only (Figure 3o). This suggested that **CyCu1** responded to the exogenously-added Cu^{2+} and a large proportion of **CyCu1** was converted to CyK1.

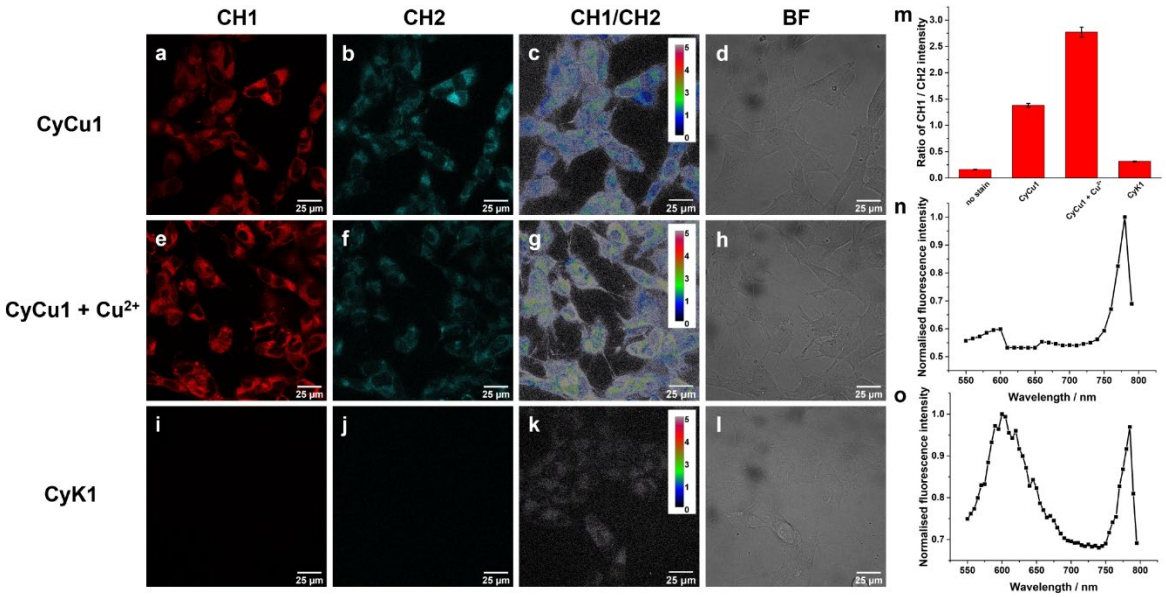

Figure 3. Representative confocal microscopy images of SH-SY5Y cells that were incubated in different conditions at 37 °C. Three channels were collected. CH1: 523 nm laser, 580–650 nm emission; CH2: MP840 nm laser, 750–800 nm emission; Brightfield (BF): 488 nm laser. CH1/CH2 refers to the ratio image of CH1 and CH2. (a–d) Cells were treated with **CyCu1** (10 μM) for 1 h. (e–h) Cells were pretreated with Cu^{2+}(ATSM) (10 μM) for 1 h, followed by incubation with **CyCu1** (10 μM) for 1 h. (i–l) Cells were treated with CyK1 (10 μM) for 1 h. (m) Ratio of the quantified fluorescence intensity in CH1 and CH2. Error bar stands for standard error of the mean (S.E.M.). (n) Emission spectral scan of cells treated with **CyCu1** (10 μM) for 1 h using a MP840 nm laser. (o) Emission spectral scan of cells pretreated with Cu^{2+}(ATSM) (10 μM) for 1 h and subsequently treated with **CyCu1** (10 μM) for 1 h using a MP840 nm laser.

Imaging of Cu^{2+} in Arabidopsis. In addition to using **CyCu1** to assess the copper changes in neurological disease, we were keen to determine whether it could be used in non-mammalian systems. In this case, we wanted to investigate plants, as copper imbalances, whether excess or deficiency, are detrimental to growth.[34] Arabidopsis

is commonly used for the investigation of metal uptake through root systems.[35] **CyCu1** was applied to detect exogenous Cu^{2+} in the root of wild-type Arabidopsis. Arabidopsis seedlings were stained with **CyCu1** with and without Cu^{2+} for 1 h, and the root tips were imaged. In the seedling that stained with **CyCu1**, negligible fluorescence was observed in the product channel and bright fluorescence was detected in the probe channel, showing that **CyCu1** was able to penetrate through the cell wall and membrane, and endogenous Cu^{2+} was not detected in the root tip (Figure S15a–d). In contrast, in the presence of exogenous Cu^{2+}, increased fluorescence in the product channel and decreased fluorescence in the probe channel were observed, indicating a 16-fold greater Cu^{2+} content when compared with the seedling without exogenous Cu^{2+} incubation (Figure S15e–h, m). The permeability of CyK1 was also examined. The seedling that stained with CyK1 was non-fluorescent in both probe and product channels, verifying that CyK1 was not cell permeable (Figure S15i–l). This result was consistent with the imaging study of SH-SY5Y cells. CyK1 was not able to penetrate through either the membrane of SH-SY5Y cells or the cell wall of Arabidopsis root. The result demonstrated that **CyCu1** was able to detect exogenous Cu^{2+} in the root of Arabidopsis, and the probe is therefore a potential tool for the investigation of Cu^{2+} homeostasis in plants. This is significant because the majority of reported fluorescent probes are only reported in mammalian systems, and there is therefore little information about features of organic probes that are suitable for imaging of plants and other systems.[36]

Imaging of Cu^{2+} in neuroblastoma tumors. For the tissue study we used tumor tissue derived from the neuroblastoma Th-MYCN mouse model previously published by our collaborator.[37] We tested samples derived from control mice and mice treated orally with 400 mg/kg of the copper chelator tetraethylenepentamine (TEPA) for one week. The tissue in the control group was extracted from mice with neuroblastoma tumors, which has previously been reported to have higher copper levels.[13] In contrast, the tissue in the chelator treated group was extracted from mice fed with the copper chelator as a treatment for neuroblastoma, and it was therefore expected to have less free copper.

The two types of tissue sections were first stained with DAPI to visualize cell nuclei, followed by staining with **CyCu1** for 1 h. Intense fluorescence in the product channel (CH1) and negligible fluorescence in the probe channel (CH2) were observed in the control group (Figure 4a–e), consistent with high Cu^{2+} content in neuroblastoma tumors. In the chelator treated group, an opposite trend was observed. Negligible fluorescence was observed in the product channel and significant fluorescence was observed in the probe channel (Figure 4f–j), consistent with the absence of Cu^{2+} in the tissue section. The ratio of the fluorescence intensity in CH1 and CH2 showed a 140-fold higher ratio in the control tissue (Figure 4k). This result is consistent with the finding that total copper levels in neuroblastoma tumors is higher than that of chelator-treated tissue.[13] Importantly, the imaging study reveals that labile Cu^{2+} is present in the neuroblastoma tumor tissue, while previous reports were able to measure only total copper levels, without selectivity for labile Cu^{2+} pool. This is the first report of the detection of endogenous labile Cu^{2+} in neuroblastoma tumors.

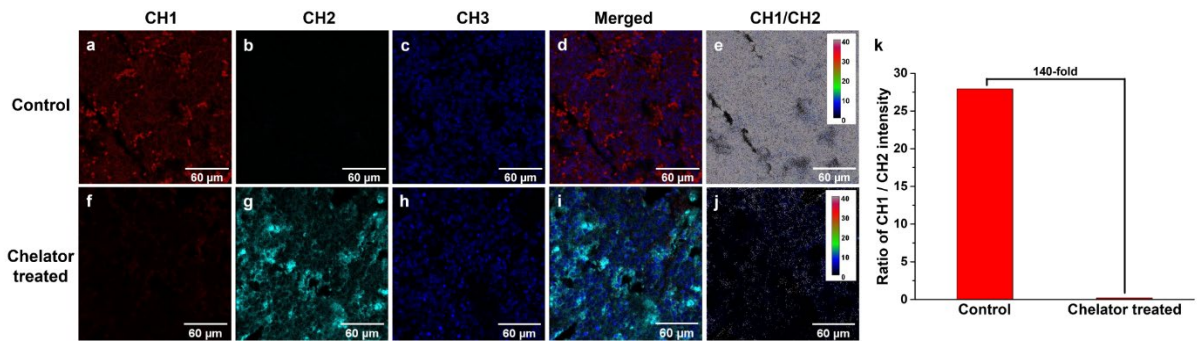

Figure 4. Two types of tissue sections were stained with DAPI (10 μM) in PBS buffer (1x, pH 7.4) at rt for 10 min, and then stained with **CyCu1** (20 μM) in HEPES buffer (20 mM, pH 7.4, containing 0.2% DMSO and 0.1% CrEL as cosolvents, v/v) at rt for 1 h. Fluorescence images were captured in three channels. CH1 for product: 535 nm laser, 580–650 nm emission; CH2 for probe: MP840 nm laser, 750–800 nm emission; CH3 for DAPI: 760 nm multiphoton laser, 400–470 nm emission. CH1, CH2 and CH3 were merged. CH1/CH2 refers to the ratio image of CH1 and CH2. (a–e) Representative images of the control tissue. (f–j) Representative images of the chelator treated tissue. (k) Ratio of the quantified fluorescence intensity in CH1 and CH2.

Imaging of Cu^{2+} in DLB. After demonstrating that **CyCu1** has the ability to detect endogenous Cu^{2+} in neuroblastoma tumor tissues, we were interested in investigating the distribution and level of Cu^{2+} in human brain tissue from patients with the Lewy body disease, DLB. In this work, Cu^{2+} levels were regionally examined in a brain region that experiences marked degeneration in DLB, the SN[38], and compared with tissues from the same region in healthy age-matched control brains. Tissue sections were incubated with **CyCu1** for 1 h prior to fluorescence imaging. Higher intensity in CH1, and lower intensity in CH2, corresponds to higher Cu^{2+} levels. One of the merits of fluorescence imaging is its non-destructive nature; this allowed us to analyze Cu^{2+} content in different tissue regions, such as individual neurons and extraneuronal space, and represents a significant advantage over quantification of copper using a destructive method, such as ICP-MS. In all SN sections, neurons exhibiting pigmented morphology (melanized dopaminergic neurons) and extraneuronal space were chosen for the analysis. Within individual dopaminergic neurons, the cytoplasm containing dark-colored neuromelanin could be clearly differentiated from the cell nuclei. Cu^{2+} content of nuclei, cytoplasm and whole cell (individual neurons) were quantified separately. For all tissue compartments, Cu^{2+} levels in DLB SN were significantly reduced (Figure 5e–h, i) compared with the same tissue compartment in the control SN (Figure 5a–d, i). Image ratios demonstrated that, within individual neurons the distribution of Cu^{2+} was heterogeneous with higher Cu^{2+} level in the nuclei and lower Cu^{2+} levels in the cytoplasm (Figure 5d, h). This is the first report of decreased Cu^{2+} in the vulnerable SN in DLB and is consistent with the marked reduction in copper previously reported in the SN in Parkinson disease.[39] This is also the first report of variable Cu^{2+} levels in neuronal nuclei and cytoplasm in Lewy body disease. Our finding enhances the understanding of a possible role for copper in DLB.

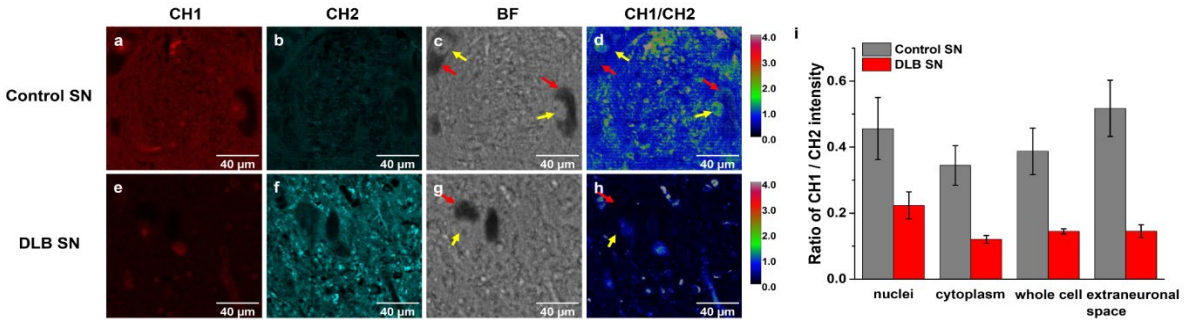

Figure 5. SN tissue sections were stained with **CyCu1** (20 μM) in HEPES buffer (20 mM, pH 7.4, containing 0.2% DMSO and 0.1% CrEL as cosolvents, v/v) at rt for 1 h. CH1 for product: 535 nm laser, 580–650 nm emission; CH2 for probe: MP840 nm laser, 750–800 nm emission; Brightfield (BF): 488 nm laser. CH1/CH2 refers to the ratio image of CH1 and CH2. (a–d) Representative images of control SN. (e–h) Representative images of DLB SN. (i) Ratio of quantified fluorescence intensity in CH1 and CH2 in nuclei, cytoplasm, whole cell and extraneuronal space of control SN and DLB SN. Error bar represents S.E.M.. Yellow arrow: nucleus; red arrow: cytoplasm.

Preliminary fluorescence and photoacoustic imaging. Having demonstrated that **CyCu1** was able to detect Cu^{2+} in the biological samples, we evaluated the capability of **CyCu1** in fluorescence and photoacoustic imaging using *in vivo* imaging systems, to determine if **CyCu1** is suitable for *in vivo* studies. Solutions of **CyCu1** with and without added Cu^{2+} in the HEPES buffer were placed on the stage of *in vivo* fluorescence imaging system. The fluorescence images were captured in two channels: one with a 745 nm excitation filter and an 820 nm emission filter for the probe, another with a 535 nm excitation filter and a 600 nm emission filter for the product. In the probe channel, **CyCu1** gave a strong fluorescence emission while **CyCu1** with addition of Cu^{2+} showed negligible fluorescence (Figure 6b). In the product channel, **CyCu1** with added Cu^{2+} exhibited a strong emission, but **CyCu1** gave no fluorescence signal (Figure 6a). This was consistent with the emission spectral change upon response to Cu^{2+} in the fluorometer study. The fluorescence images were quantified and the ratio of the radiance between the two channels was then calculated (Figure 6d). The addition of Cu^{2+} to **CyCu1** resulted in a more than 200-fold ratio increase, indicating that **CyCu1** was able to detect Cu^{2+} in a ratiometric manner in *in vivo* imaging.

Photoacoustic imaging combines optical excitation and ultrasound detection, and has advantages for *in vivo* studies.[40] It uses a pulsed laser to irradiate endogenous or exogenous contrast agents. The irradiation energy is absorbed by the contrast agent, leading to transient local thermoelastic expansion of the surrounding tissue. The thermal expansion induces pressure fluctuations that propagate through tissue, which can be detected as ultrasound waves and digitalized to construct a three-dimensional image of the tissue.[41] Photoacoustic imaging causes less photo-damage to tissue and the scattering of ultrasound waves in tissue is two to three orders of magnitude weaker than optical scattering.[42] Less dissipation of the ultrasound signal enables high spatial resolution imaging and deep tissue penetration of several centimeters.[43] To emit a photoacoustic signal, the contrast agent requires an absorption within the irradiation window, usually 680–950 nm on commercial photoacoustic imaging instruments. The variation in absorption intensity or wavelength is the requirement for sensing analytes. **CyCu1** showed a strong photoacoustic signal at 760 nm (Figure 6c). In contrast, CyK1 gave no photoacoustic signal at this wavelength (Figure 6c). Upon addition of Cu^{2+}, **CyCu1** showed a more than ten times decrease in photoacoustic signal (Figure 6c, e), consistent with the reduced absorbance at 760 nm in response to Cu^{2+}. A photoacoustic spectral scan showed that **CyCu1** exhibited a maximum photoacoustic signal at 760 nm, while CyK1 and **CyCu1** in the presence of Cu^{2+} gave no photoacoustic signal beyond 680 nm (Figure S15). The results suggested that **CyCu1** is suitable for photoacoustic imaging of Cu^{2+} with a turn-off response.

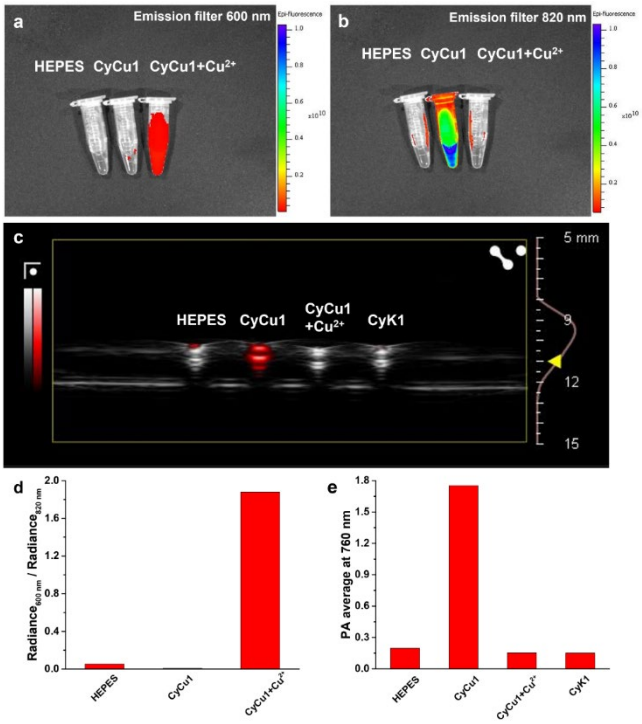

Figure 6. (a, b) Solutions of a blank control and the probe in Eppendorf tubes were placed from left to right: HEPES buffer, **CyCu1** (5 μM), **CyCu1** (5 μM) with addition of ten equivalents of Cu^{2+} in HEPES buffer (20 mM, pH 7.4, containing 0.5% DMSO and 0.1% CrEL as cosolvents, v/v). Fluorescence images were captured (a) in the product channel with a 535 nm excitation filter and a 600 nm emission filter and (b) in the probe channel with a 745 nm excitation filter and an 820 nm emission filter. (c) The solutions were placed in capillary tubes from left to right: HEPES buffer, **CyCu1** (5 μM), **CyCu1** (5 μM) with ten equivalents of Cu^{2+} and CyK1 (5 μM) in the HEPES buffer. The photoacoustic image was captured at 760 nm and merged with the ultrasound image. (d) Ratio of the radiance intensity between 600 nm and 820 nm emission channels. (e) Average photoacoustic intensity at 760 nm.

CONCLUSION

In summary, we have developed a reaction-based NIR ratiometric fluorescent probe, **CyCu1,** for Cu^{2+} based on a cyanine scaffold. 2-Picolinate ester was the sensing group and installed onto the cyclohexene moiety in the cyanine scaffold. Cu^{2+} promotes the hydrolysis of 2-picolinate ester in **CyCu1**, resulting in changes in both fluorescence emission and absorption with a more than 200 nm shift. **CyCu1** had good stability in aqueous solution and exhibited high selectivity for Cu^{2+} over other metals. **CyCu1** ratiometrically detected Cu^{2+} in several biological models using confocal microscopy. The probe not only detected exogenous Cu^{2+} in SH-SY5Y cells and Arabidopsis roots, but also was able to distinguish chelator-treated neuroblastoma tumor tissue from control tissue based on Cu^{2+} content. Our work reports on the detection of endogenous labile Cu^{2+} in neuroblastoma tumor for the first time. We also investigated Cu^{2+} content in human DLB brain tissues compared with healthy control tissues using **CyCu1** and the fluorescence imaging revealed reduced Cu^{2+} levels in the degenerating SN in this disorder. This non-destructive imaging method allowed us to distinguish the Cu^{2+} content of different tissue components. Within individual neurons, DLB SN exhibited less Cu^{2+} in nuclei, cytoplasm and the whole cell, compared with control SN. This is the first report of decreased Cu^{2+} level in the degenerating SN in DLB and supports a body of literature reporting decreased copper in the SN in Parkinson disease. Our probe may represent a useful tool for the investigation of Cu^{2+} dyshomeostasis in neurological disorders and support the development of therapies for these diseases. Our probe also showed potential for operating in dual-modality

fluorescent/photoacoustic imaging of Cu^{2+} in *in vivo* studies.

AUTHOR INFORMATION

Corresponding Author

Elizabeth J. New – School of Chemistry; Sydney Nano Institute; Australian Research Council Centre of Excellence for Innovations in Peptide and Protein Science, The University of Sydney, Sydney, NSW, 2006, Australia

Authors

Jianping Zhu – School of Chemistry, The University of Sydney, Sydney, NSW, 2006, Australia; Currently at Janelia Research Campus, Howard Hughes Medical Institute, Ashburn, VA, 20147, United States

Marcus E. Graziotto – School of Chemistry, The University of Sydney, Sydney, NSW, 2006, Australia

Veronica Cottam – Brain and Mind Centre and School of Medical Sciences (Neuroscience), The University of Sydney, Sydney, NSW, 2006, Australia.

Tom Hawtrey – School of Chemistry; Sydney Nano Institute; Australian Research Council Centre of Excellence for Innovations in Peptide and Protein Science, The University of Sydney, Sydney, NSW, 2006, Australia

Jourdin R. C. Rouaen – Children's Cancer Institute, Lowy Cancer Research Centre, UNSW Sydney, Randwick, New South Wales, Australia

Carolyn Ohno – School of Life and Environmental Sciences, The University of Sydney, Sydney, NSW, 2006, Australia

Marcus Heisler – School of Life and Environmental Sciences, The University of Sydney, Sydney, NSW, 2006, Australia

Orazio Vittorio – Children's Cancer Institute, Lowy Cancer Research Centre, UNSW Sydney, Randwick, New South Wales, Australia; School of Biomedical Sciences, University of New South Wales, Kensington, NSW, 2031, Australia

Kay L. Double – Brain and Mind Centre and School of Medical Sciences (Neuroscience), The University of Sydney, Sydney, NSW, 2006, Australia.

Notes

All authors have given approval to the final version of the manuscript.

ACKNOWLEDGMENTS

The authors would like to acknowledge the Australian Research Council (CE200100012, DP210102148) and the Human Frontier Science Program (RGP0060/2021) for funding (E.J.N.), the University of Sydney International Stipend Scholarship (J.Z.), the China Scholarship Council for a PhD Scholarship (J.Z.) and the Australian Government for Research Training Program Scholarships (M.G.). We acknowledge the scientific and technical assistance of the Australian Microscopy and Microanalysis Research Facility at the Australian Centre for Microscopy and Microanalysis (ACMM). We acknowledge the support received from the preclinical facilities at Sydney Imaging. The authors thank the staff of The London Neurodegenerative Diseases Brain Bank which receives funding from the MRC and as part of the Brains for Dementia Research programme, jointly funded by Alzheimer's Research UK and Alzheimer's Society.

REFERENCES

1. Prashanth, L.; Kattapagari, K. K.; Chitturi, R. T.; Baddam, V. R. R.; Prasad, L. K., A Review on Role of Essential Trace Elements in Health and Disease. *J. NTR Univ. Health Sci.* **2015,** *4* (2), 75-85.

2. Gromadzka, G.; Tarnacka, B.; Flaga, A.; Adamczyk, A., Copper Dyshomeostasis in Neurodegenerative Diseases-Therapeutic Implications. *Int. J. Mol. Sci.* **2020,** *21* (23), 9259.

3. Bulcke, F.; Dringen, R.; Scheiber, I. F., Neurotoxicity of Metals In *Neurotoxicity of Metals. Advances in Neurobiology*, Aschner, M.; Costa, L., Eds. Springer: Cham., 2017; Vol. 18, pp 313–343.

4. Scholefield, M.; Church, S. J.; Xu, J.; Patassini, S.; Roncaroli, F.; Hooper, N. M.; Unwin, R. D.; Cooper, G. J. S., Widespread Decreases in Cerebral Copper Are Common to Parkinson's Disease Dementia and Alzheimer's Disease Dementia. *Front. Aging Neurosci.* **2021,** *13*, 641222.

5. (a)Davies, K. M.; Hare, D. J.; Cottam, V.; Chen, N.; Hilgers, L.; Halliday, G.; Mercer, J. F. B.; Double, K. L., Localization of Copper and Copper Transporters in the Human Brain. *Metallomics* **2012,** *5* (1), 43-51; (b)Krebs, N.; Langkammer, C.; Goessler, W.; Ropele, S.; Fazekas, F.; Yen, K.; Scheurer, E., Assessment of Trace Elements in Human Brain Using Inductively Coupled Plasma Mass Spectrometry. *J. Trace Elem. Med. Biol.* **2014,** *28* (1), 1-7.

6. Davies, K. M.; Bohic, S.; Carmona, A.; Ortega, R.; Cottam, V.; Hare, D. J.; Finberg, J. P. M.; Reyes, S.; Halliday, G. M.; Mercer, J. F. B.; Double, K. L., Copper Pathology in Vulnerable Brain Regions in Parkinson's Disease. *Neurobiol. Aging* **2014,** *35* (4), 858-866.

7. Deibel, M. A.; Ehmann, W. D.; Markesbery, W. R., Copper, Iron, and Zinc Imbalances in Severely Degenerated Brain Regions in Alzheimer's Disease: Possible Relation to Oxidative Stress. *J. Neurol. Sci.* **1996,** *143* (1), 137-142.

8. Lovell, M. A.; Robertson, J. D.; Teesdale, W. J.; Campbell, J. L.; Markesbery, W. R., Copper, Iron and Zinc in Alzheimer's Disease Senile Plaques. *J. Neurol. Sci.* **1998,** *158* (1), 47-52.

9. McKeith, I. G.; Boeve, B. F.; Dickson, D. W., Diagnosis and Management of Dementia with Lewy Bodies: Fourth Consensus Report of the DLB Consortium *Neurology* **2017,** *89* (1), 88-100.

10. (a)Boot, B. P.; McDade, E. M.; McGinnis, S. M.; Boeve, B. F., Treatment of Dementia with Lewy Bodies. *Curr. Treat. Options Neurol.* **2013,** *15* (6), 738-764; (b)Taylor, J. P.; McKeith, I. G.; Burn, D. J.; Boeve, B. F.; Weintraub, D.; Bamford, C.; Allan, L. M.; Thomas, A. J.; O'Brien, J. T., New Evidence on the Management of Lewy Body Dementia. *Lancet Neurol.* **2020,** *19* (2), 157-169.

11. Matthay, K. K.; George, R. E.; Yu, A. L., Promising Therapeutic Targets in Neuroblastoma *Clin. Cancer Res.* **2012,** *18* (10), 2740-2753.

12. Vittorio, O.; Brandl, M.; Cirillo, G.; Kimpton, K.; Hinde, E.; Gaus, K.; Yee, E.; Kumar, N.; Duong, H.; Fleming, C.; Haber, M.; Norris, M.; Boyer, C.; Kavallaris, M., Dextran-Catechin: An Anticancer Chemically-Modified Natural Compound Targeting Copper That Attenuates Neuroblastoma Growth. *Oncotarget* **2016,** *7* (30), 47479-47493.

13. Parmar, A.; Pascali, G.; Voli, F.; Lerra, L.; Yee, E.; Ahmed-Cox, A.; Kimpton, K.; Cirillo, G.; Arthur, A.; Zahra, D.; Rahardjo, G.; Liu, G. J.; Lengkeek, N.; Saletta, F.; Charil, A.; Kavallaris, M.; Vittorio, O., In Vivo [^{64}Cu]$CuCl_2$ PET Imaging Reveals Activity of Dextran-Catechin on Tumor Copper Homeostasis. *Theranostics* **2018,** *8* (20), 5645-5659.

14. Bohic, S.; Murphy, K.; Paulus, W.; Cloetens, P.; Salomé, M.; Susini, J.; Double, K., Intracellular Chemical Imaging of the Developmental Phases of Human Neuromelanin Using Synchrotron X-ray Microspectroscopy. *Anal. Chem.* **2008,** *80* (24), 9557-9566.

15. Lutsenko, S., Dynamic and Cell-specific Transport Networks for Intracellular Copper Ions. *J. Cell Sci.* **2021,** *134* (21), jcs240523.

16. Lin, C.; Zhang, Z.; Wang, T.; Chen, C.; James Kang, Y., Copper Uptake by DMT1: A Compensatory Mechanism for CTR1 Deficiency in Human Umbilical Vein Endothelial Cells. *Metallomics* **2015,** *7* (8), 1285-1289.

17. Lee, J.; Peña, M. M.; Nose, Y.; Thiele, D. J., Biochemical Characterization of the Human Copper Transporter Ctr1. *J. Biol. Chem.* **2002,** *277* (6), 4380-4387.

18. Pezacki, A. T.; Matier, C. D.; Gu, X.; Kummelstedt, E.; Bond, S. E.; Torrente, L.; Jordan-Sciutto, K. L.; DeNicola, G. M.; Su, T. A.; Brady, D. C.; Chang, C. J., Oxidation State-Specific Fluorescent Copper Sensors Reveal Oncogene-Driven Redox Changes That Regulate Labile Copper(II) Pools. *Proc. Natl. Acad. Sci. U. S. A.* **2022,** *119* (43), e2202736119.

19. Tamil Selvan, G.; Varadaraju, C.; Tamil Selvan, R.; Enoch, I. V. M. V.; Mosae Selvakumar, P., On/Off Fluorescent Chemosensor for Selective Detection of Divalent Iron and Copper Ions: Molecular Logic Operation and Protein Binding. *ACS Omega* **2018,** *3* (7), 7985-7992.

20. (a)Pearson, R. G., Hard and Soft Acids and Bases. *J. Am. Chem. Soc.* **1963,** *85* (22), 3533-3539; (b)Pearson, R. G., Hard and Soft Acids and Bases, HSAB, Part 1: Fundamental Principles. *J. Chem. Educ.* **1968,** *45* (9), 581-587.

21. Yuan, L.; Lin, W.; Zheng, K.; He, L.; Huang, W., Far-red to Near Infrared Analyte-responsive Fluorescent Probes Based on Organic Fluorophore Platforms for Fluorescence Imaging. *Chem. Soc. Rev.* **2013,** *42* (2), 622-661.

22. Lee, M. H.; Kim, J. S.; Sessler, J. L., Small Molecule-based Ratiometric Fluorescence Probes for Cations, Anions, and Biomolecules. *Chem. Soc. Rev.* **2015,** *44* (13), 4185-4191.

23. (a)Huang, Y.; Li, C.-F.; Shi, W.-J.; Tan, H.-Y.; He, Z.-Z.; Zheng, L.; Liu, F.; Yan, J.-W., A Near-infrared BODIPY-based Fluorescent Probe for Ratiometric and Discriminative Detection of Hg2+ and Cu2+ Ions in Living Cells. *Talanta* **2019,** *198*, 390-397; (b)Aydin, Z.; Yan, B.; Wei, Y.; Guo, M., A Novel Near-infrared Turn-on and Ratiometric Fluorescent Probe Capable of Copper(ii) Ion Determination in Living Cells. *Chem. Commun.* **2020,** *56* (45), 6043-6046; (c)Guo, R.; Wang, Q.; Lin, W., A Ratiometric and Near-infrared Fluorescent Probe for Imaging Cu2+ in Living Cells and Animals. *J. Fluoresc.* **2017,** *27*, 1655–1660.

24. Fife, T. H.; Przystas, T. J., Divalent Metal Ion Catalysis in the Hydrolysis of Esters of Picolinic Acid. Metal Ion Promoted Hydroxide Ion and Water Catalyzed Reactions. *J. Am. Chem. Soc.* **1985,** *107* (4), 1041-1047.

25. Li, H.; Zhang, P.; Smaga, L. P.; Hoffman, R. A.; Chan, J., Photoacoustic Probes for Ratiometric Imaging of Copper(II). *J. Am. Chem. Soc.* **2015,** *137* (50), 15628-15631.

26. (a)Jiang, J.; Sun, H.; Hu, Y.; Lu, G.; Cui, J.; Hao, J., AIE + ESIPT Activity-based NIR Cu^{2+} Sensor with Dye Participated Binding Strategy. *Chem. Commun.* **2021,** *57* (62), 7685-7688; (b)Zhu, D.; Luo, Y.; Shuai, L.; Xie, W.; Yan, X.; Duan, Z.; Cai, W., A Hemicyanine-based Selective and Sensitive Colorimetric and Fluorescent Turn-on Probe for Cu^{2+}. *Tetrahedron Lett.* **2016,** *57* (48), 5326-5329.

27. Yi, X.; Yan, F.; Wang, F.; Qin, W.; Wu, G.; Yang, X.; Shao, C.; Chung, L. W.; Yuan, J., IR-780 Dye for Near-Infrared Fluorescence Imaging in Prostate Cancer. *Med. Sci. Monit.* **2015,** *21*, 511-517.

28. Yuan, L.; Lin, W.; Yang, Y., A Ratiometric Fluorescent Probe for Specific Detection of Cysteine over Homocysteine and Glutathione Based on the Drastic Distinction in the Kinetic Profiles. *Chem. Commun.* **2011,** *47* (22), 6275-6277.

29. Gupte, A.; Mumper, R. J., Elevated Copper and Oxidative Stress in Cancer Cells as A Target for Cancer Treatment. *Cancer Treat. Rev.* **2009,** *35* (1), 32-46.

30. Parmar, A.; Pascali, G.; Voli, F.; Lerra, L.; Yee, E.; Ahmed-Cox, A.; Kimpton, K.; Cirillo, G.; Arthur, A.; Zahra, D.; Rahardjo, G.; Liu, G. J.; Lengkeek, N.; Saletta, F.; Charil, A.; Kavallaris, M.; Vittorio, O., In vivo [(64)Cu]CuCl2 PET imaging reveals activity of Dextran-Catechin on tumor copper homeostasis. *Theranostics* **2018,** *8* (20), 5645-5659.

31. (a)Kovalevich, J.; Langford, D., Considerations for the Use of SH-SY5Y Neuroblastoma Cells in Neurobiology. *Methods Mol. Biol.* **2013,** *1078*, 9-21; (b)Xicoy, H.; Wieringa, B.; Martens, G. J. M., The SH-SY5Y Cell Line in Parkinson's Disease Research: a Systematic Review. *Mol. Neurodegener.* **2017,** *12* (1), 10.

32. Djoko, K. Y.; Paterson, B. M.; Donnelly, P. S.; McEwan, A. G., Antimicrobial Effects of Copper(II) Bis(thiosemicarbazonato) Complexes Provide New Insight into Their Biochemical Mode of Action. *Metallomics* **2014,** *6* (4), 854-863.

33. Jones, S., Permeability Rules for Antibiotic Design. *Nat. Biotechnol.* **2017,** *35* (7), 639.
34. Mandal, S.; Gupta, S. K.; Ghorai, M.; Patil, M. T.; Biswas, P.; Kumar, M.; Radha; Gopalakrishnan, A. V.; Mohture, V. M.; Rahman, M. H.; Prasanth, D. A.; Mane, A. B.; Jha, N. K.; Jha, S. K.; Lal, M. K.; Tiwari, R. K.; Dey, A., Plant Nutrient Dynamics: A Growing Appreciation for the Roles of Micronutrients. *Plant Growth Regul.* **2023,** *100* (2), 435-452.
35. (a)Kajala, K.; Walker, K. L.; Mitchell, G. S.; Krämer, U.; Cherry, S. R.; Brady, S. M., Real-Time Whole-Plant Dynamics of Heavy Metal Transport in Arabidopsis Halleri and Arabidopsis Thaliana by Gamma-ray Imaging. *Plant Direct* **2019,** *3* (4), e00131; (b)Shanmugam, V.; Lo, J. C.; Yeh, K. C., Control of Zn Uptake in Arabidopsis Halleri: A Balance between Zn and Fe. *Front. Plant Sci.* **2013,** *4*, 281.
36. Hawtrey, T.; New, E. J., Molecular Probes for Fluorescent Sensing of Metal Ions in Non-mammalian Organisms. *Curr. Opin. Chem. Biol.* **2023,** *74*, 102311.
37. Voli, F.; Valli, E.; Lerra, L.; Kimpton, K.; Saletta, F.; Giorgi, F. M.; Mercatelli, D.; Rouaen, J. R. C.; Shen, S.; Murray, J. E.; Ahmed-Cox, A.; Cirillo, G.; Mayoh, C.; Beavis, P. A.; Haber, M.; Trapani, J. A.; Kavallaris, M.; Vittorio, O., Intratumoral Copper Modulates PD-L1 Expression and Influences Tumor Immune Evasion. *Cancer Res.* **2020,** *80* (19), 4129-4144.
38. (a)Donaghy, P. C.; McKeith, I. G., The Clinical Characteristics of Dementia with Lewy Bodies and a Consideration of Prodromal Diagnosis. *Alzheimer's Res. Ther.* **2014,** *6*, 46; (b)Outeiro, T. F.; Koss, D. J.; Erskine, D.; Walker, L.; Kurzawa-Akanbi, M.; Burn, D.; Donaghy, P.; Morris, C.; Taylor, J. P.; Thomas, A.; Attems, J.; McKeith, I., Dementia with Lewy Bodies: An Update and Outlook. *Mol. Neurodegener.* **2019,** *14* (1), 5.
39. Genoud, S.; Senior, A. M.; Hare, D. J.; Double, K. L., Meta-Analysis of Copper and Iron in Parkinson's Disease Brain and Biofluids. *Mov Disord* **2020,** *35* (4), 662-671.
40. (a)Attia, A. B. E.; Balasundaram, G.; Moothanchery, M.; Dinish, U. S.; Bi, R.; Ntziachristos, V.; Olivo, M., A Review of Clinical Photoacoustic Imaging: Current and Future Trends. *Photoacoustics* **2019,** *16*, 100144; (b)Banala, S.; Fokong, S.; Brand, C.; Andreou, C.; Kräutler, B.; Rueping, M.; Kiessling, F., Quinone-Fused Porphyrins as Contrast Agents for Photoacoustic Imaging. *Chem. Sci.* **2017,** *8* (9), 6176-6181.
41. Fu, Q.; Zhu, R.; Song, J.; Yang, H.; Chen, X., Photoacoustic Imaging: Contrast Agents and Their Biomedical Applications. *Adv. Mater.* **2019,** *31* (6), e1805875.
42. Nyayapathi, N.; Xia, J., Photoacoustic Imaging of Breast Cancer: A Mini Review of System Design and Image Features. *J. Biomed. Opt.* **2019,** *24* (12), 1-13.
43. (a)Knox, H. J.; Chan, J., Acoustogenic Probes: A New Frontier in Photoacoustic Imaging. *Acc. Chem. Res.* **2018,** *51* (11), 2897-2905; (b)Zhang, Y.; Hong, H.; Cai, W., Photoacoustic Imaging. *Cold Spring Harb Protoc.* **2011,** *2011* (9).